MULTILAYER GRATINGS FOR X-UV OPTICS[*]

M. Jergel, P. Mikulík[1] , E. Majková, E. Pinčík, Š. Luby
Institute of Physics, Slovak Academy of Sciences, Dúbravská cesta 9, 842 28 Bratislava,
Slovakia

M. Brunel
Laboratoire de Cristallographie du CNRS, B.P. 166, 38042 Grenoble Cedex 09, France

P. Hudek, I. Kostič
Institute of Computer Systems, Slovak Academy of Sciences, Dúbravská cesta 9, 842 37
Bratislava, Slovakia

Multilayer gratings are thin film structures possessing periodicities both in the normal and lateral directions. They combine the properties of surface gratings and planar multilayers thus providing a high throughput and high spectral resolution on higher diffraction orders. The unique diffraction properties are utilized in the X-ray and ultraviolet optics where no lenses or mirrors comparable with those for visible light are available. Multilayer gratings act as constant resolution dispersion elements in a broad spectral range. A fan of grating diffractions in real space is represented by a set of points on equidistant truncation rods in the reciprocal space. The kinematical theory of X-ray scattering explains well the positions of the grating truncation rods while the dynamical theory is inevitable to calculate the intensities along the truncation rods (grating efficiency). The properties of multilayer gratings are exemplified on two differently prepared lamellar gratings with the nominal normal and lateral periods of 8 nm and 800 nm, respectively. The fabrication steps are described in detail. The specular and non-specular X-ray reflectivities at wavelength 0.15418 nm were measured on one of the samples. The dynamical theory of X-ray scattering with a matrix modal eigenvalue approach was applied to extract the real structural parameters such as the surface and interface roughnesses, individual layer thicknesses, and the lamella width to the grating period ratio. The X-ray reflectometry is completed by microscopy observations which provide complementary and direct information on the local surface profile.

---

[*]Presented at the Workshop on Solid State Surfaces and Interfaces II, Bratislava, Slovakia, June 20 – 22, 2000.
[1]also Laboratory of Thin Films and Nanostructures, Faculty of Science, Masaryk University, Kotlářská 2, 611 37 Brno, Czech Republic.

1   Introduction

Multilayer structures have become increasingly important with the development of optical elements for the soft X-ray (0.4 – 12.5 nm) and extreme ultraviolet (EUV) (12.5 – 80 nm) region which has been stimulated by new applications in plasma source diagnostics, astronomy, projection lithography, soft X-ray microscopy, beamline optics at synchrotron storage rings, etc. The use of multilayers is inevitable due to the absence of mirrors and lenses comparable with those for visible light in the X-UV region. Here the refractive index is less than unity and penetration depth is much larger than for visible light so that normal-incidence reflectivity of materials goes down rapidly. On the other hand, natural crystals have the lattice parameters too small for the X-UV region. Therefore normal-incidence reflective optics based on multilayer mirrors is used in this wavelength range. Multilayer mirrors are preferred to natural crystal monochromators even for hard X-rays if the intensity is more important than resolution for a given type of experiment. Here grazing incidence geometry must be applied.

A multilayer mirror works on the principle of constructive interference of the waves reflected from regularly displaced interfaces between the layers of a heavy metal (refractor) and a light element (spacer) which alternate in a regular way [1]. These reflections are intense enough only at the incidence angles close to the critical value for the total external reflection which is several tens and tenths of degree for soft and hard X-rays, respectively. The basic bilayer thickness is the period of this artificial one-dimensional crystal, being adjusted at will during the deposition. Sophisticated deposition methods with *in situ* control of the soft X-ray reflectivity of the growing multilayer to keep precisely its periodicity were developed [2].

A planar multilayer acts as a broad bandpass filter due to a limited number of multilayer periods. A rather poor spectral resolution may pose a problem in some applications. Therefore multilayer gratings (MLGs) have been preferably used which combine a high throughput with a high spectral resolution on higher diffraction orders.
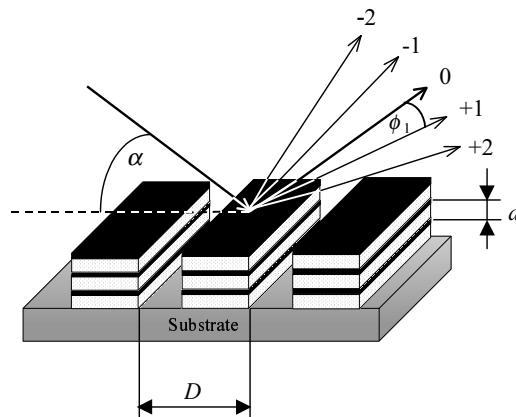
Fig. 1. A schematic view of a multilayer grating. D and d are the grating (lateral) and multilayer (normal) periods, respectively, the former being directed along the lamella surfaces and the latter perpendicularly to them. Because of clarity, the picture dimensions are not in the true proportions (see the text). The incoming X-ray beam is simultaneously diffracted into a fan of grating diffractions around the specularly reflected X-ray beam. The sign of grating diffractions is compatible with the sign of the GTRs in Fig. 2.
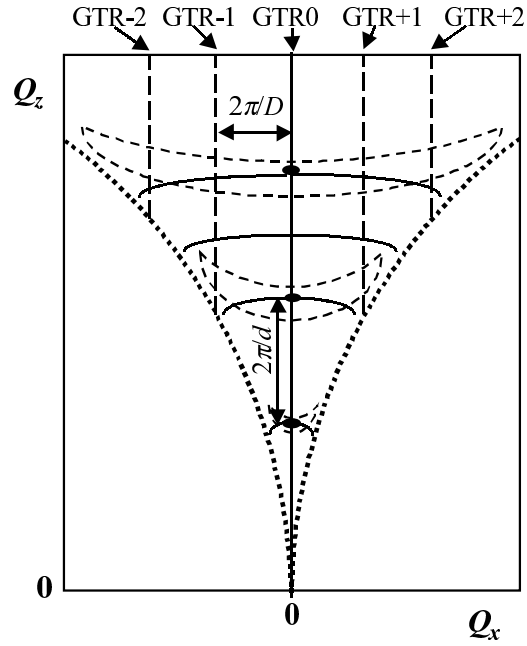
Fig. 2. The reciprocal space map. Q_x and Q_z are the lateral and normal components of the scattering vector $Q = K - K^{in}$, with K^{in} and K being the wavevectors of the incident and outgoing waves, respectively. The central full line is the specular scan trajectory along which Bragg points are located at $Q_{pz} = p(2\pi/d)$, p being an integer. Similarly, grating truncation rods (GTRs) occur at $Q_{mx} = m(2\pi/D)$, m being an integer. The full curves are rocking scan trajectories across multilayer Bragg points and in between. The former intersect the banana-shaped regions of the resonant diffuse scattering produced by conformal interfaces (see the text). The dotted curves are the limiting Ewald spheres which determine the inaccessible part of the reciprocal space in the reflection experimental geometry.

2   Grating diffraction properties

A schematic view of a multilayer grating is shown in Fig. 1. It consists of regularly displaced uniform grooves separated by lamellae with multilayer inside. The multilayer grating has two periodicities — the normal (multilayer) period d, usually of several nm, and lateral (grating) period D. Due to the present technology limitations, the minimum lateral period is about 100 nm. Comparing with a surface grating, the multilayer grating has a much higher reflectivity as the reflection takes place not only from the surface but from many interfaces. On the other hand, the spectral bandwidth is much narrower than for a planar multilayer due to the grating profile.

Now let us describe the scattering geometry. We denote K^{in} and K the wave vector of the incident beam and of a scattered beam in the vacuum, respectively. They make an angle α and β with the sample surface, respectively. A scattering event is then characterized by the scattering wave vector given by the difference between the scattered and incidence waves $Q = K - K^{in}$. Because of the lateral periodicity D of the sample, the lateral component of the scattering vector has to be an integer multiple of $2\pi/D$ (positions of grating truncation rods, GTRs, see Fig. 2).

Therefrom the grating formula follows

$$Q_{mx} = K_{mx} - K_x^{\text{in}} = \frac{2\pi}{\lambda}(\cos \beta_m - \cos \alpha) = \frac{2\pi}{D} \cdot m \tag{1}$$

which can also be interpreted in such a way that an incident wave excites the whole fan of diffracted waves whenever the angle of incidence is above a minimum value $\cos \alpha = 1 - \lambda/D$. Let us mention that the above given equation follows uniquely from the sample discrete translation symmetry irrespective of the theory used as the lateral components of the wave vectors are conserved across the interfaces. On the other hand, refraction changes the wave vector length leading to an important change of the vertical wave vector component. Refraction is neglected in the kinematical theory, thus the vertical maxima of the scattering vector in the vacuum are integer multiples of the vertical reciprocal period $2\pi/d$. Therefrom the multilayer Bragg law follows

$$Q_{pz} = K_{pz} - K_z^{\text{in}} = \frac{2\pi}{\lambda}(\sin \beta_p + \sin \alpha_p) = \frac{2\pi}{d} \cdot p \,. \tag{2}$$

Within the kinematical theory, maximum intensity at the GTR of the mth order (GTR m) is obtained for a discrete set of $\boldsymbol{Q}_{mp}$ where both the lateral and vertical resonance conditions are fulfilled. The respective incidence and exit angles are

$$p \sin \alpha_{mp} - \frac{md}{D} \cos \alpha_{mp} \;\; = \;\; \frac{\lambda p^2}{2d} + \frac{\lambda d m^2}{D^2} \tag{3}$$

$$p \sin \beta_{mp} + \frac{md}{D} \cos \beta_{mp} \;\; = \;\; \frac{\lambda p^2}{2d} + \frac{\lambda d m^2}{D^2} \,. \tag{4}$$

For the specular reflectivity where the exit angle equals the angle of incidence, thus $m = 0$ (the case to be referred further as specular scan or GTR 0 — GTR of the zeroth order), we find

$$\sin \alpha_p = \frac{\lambda}{2d} \cdot p \,. \tag{5}$$

The kinematical theory considers scattering of vacuum waves by the sample potential, thus it does not take into account the refraction. As the refractive index of X-rays is slightly less than unity, refraction is considerable until the angle of incidence equal to a multiple of the critical value. Then the vertical components of the incident, scattered and scattering vectors in the above given equations are replaced by smaller values which follow from the refraction by the averaged multilayer grating. The condition for the vertical maxima reads

$$\sqrt{(n^2 - 1) + \sin^2 \beta_p} + \sqrt{(n^2 - 1) + \sin^2 \alpha_p} = \frac{\lambda}{d} \cdot p \,. \tag{6}$$

The normal periodicity produces constructive interferences in the specular scan obeying multilayer Bragg law corrected for refraction by a multiplicative square-root term

$$p\lambda = 2d \sin \alpha_p \sqrt{1 - \frac{1 - n^2}{\sin^2 \alpha_p}} \,. \tag{7}$$

For soft X-rays it is convenient to introduce the dispersion angle $\phi_m = \alpha - \beta_m$ [3] which alternates for the exit angle β_m of a grating order m, Fig. 1. Dividing Eq. (1) by (2) we get for the kinematical positions of dispersion angles

$$\tan \frac{\phi_{mp}}{2} = \frac{dm}{Dp} \tag{8}$$

for α_{mp} fulfilling the condition (3). A procedure taking the refraction into account by evaluating ϕ_{mp} from (1) and (6) does not lead to a simple relation like that above. However, the refraction may not play a considerable role for soft X-rays and larger angles of incidence, thus (8) being a good approximation. Therefore multilayer gratings for soft X-rays have some unique diffraction properties [3]. First, the dispersion angles of enhanced grating diffractions are essentially constant with respect to the angle of incidence in a broad spectral range. Therefore multilayer gratings may be applied in the same manner as simple planar multilayers. Second, for the same reason, multilayer gratings are constant resolution dispersion elements for a given instrumental geometry. Third, multilayer gratings separate different multilayer Bragg orders, the dispersion angle being inversely proportional to the Bragg order. Fourth, for given Bragg and grating orders, the dispersion angle is determined by the ratio of the multilayer and grating periods.

3   Calculation of multilayer grating diffractions

There are interfaces of two kinds in MLGs: horizontal interfaces and vertical side walls. Their dimensions differ by two orders of magnitude. Several theories of different complexity have been developed, from a simple single-scattering kinematical theory to fully dynamical ones which properly cover refraction as well as multiple scattering features from both types of interfaces. The starting point of all of these theories is to solve the scalar wave equation for the amplitude of the electric field intensity

$$\left(\Delta + k^2(\boldsymbol{r})\right)E(\boldsymbol{r}) = 0 \, , \tag{9}$$

where $k(\boldsymbol{r}) = n(\boldsymbol{r})K$, under the condition of lateral periodicity expressed by developing the refractive index into the Fourier series

$$n(x, z) = \sum_{h} n_h(z) \, e^{ihx} \, , \tag{10}$$

where $h = 2\pi m/D$. The essential features of the diffraction pattern of multilayer gratings may be predicted by the kinematical approach to the X-ray scattering where a weak interaction with the matter is supposed: only single-scattering events from the incident wave to the scattered waves along their classical path in the sample are involved while supposing that the incident beam is not attenuated [6, 7]. The scattered intensity is then the Fourier transform of the spatial distribution of the susceptibility which may be expressed as the multiplication of the grating and multilayer periodicity functions with their corresponding structure and shape factors which provides a direct way to generalize the kinematical Fresnel reflection coefficient for the lateral diffraction case. However, the kinematical approach is unsuited to predict accurately the diffraction intensities and thus efficiency of a multilayer grating. For this, the dynamical treatment including absorption, extinction and multiple scattering effects has to be used.

There are several formulations of the dynamical theory of X-ray scattering. Here we use the modal method with the eigenvalue matrix approach [6, 7]. The wave equation (9) is solved in each homogeneous grating layer supposing a plane wave solution similar to a one-dimensional Bloch (Floquet) wave. The solution of the wave equation is transformed into an eigenvalue matrix problem, which gives the wave vector components and the Fourier coefficients of the scattered waves. Afterwards boundary conditions are applied at each interface j. This results

in the generalization of the optical Fresnel coefficients of the specular reflectivity by a planar multilayer to the lateral diffraction case of a MLG

$$(\hat{\mathfrak{r}}_j)_{mn} = \frac{k_{z,m}^{(j)} - k_{z,n}^{(j+1)}}{k_{z,m}^{(j)} + k_{z,n}^{(j+1)}} \qquad (\hat{\mathfrak{t}}_j)_{mn} = \frac{2k_{z,m}^{(j)}}{k_{z,m}^{(j)} + k_{z,n}^{(j+1)}} \ . \tag{11}$$

These coefficients relate the transmission and reflection processes to simultaneous diffraction events between the wave fields of the GTRs of the mth and nth orders. It is worth noticing that these generalized coefficients for the specular reflection $m = n = 0$ coincide with those for the optical reflection [8] when the dynamical effects of the lateral scattering are weak.

Interfaces of multilayered samples are never perfectly flat. The roughness is usually smaller than one nanometer, which is comparable to the hard X-ray wavelengths and thus it substantially influences the scattered intensity. In presence of the Gaussian roughness of horizontal interfaces with the root mean square value σ_j, the generalized Fresnel coefficients are modified as [6,7]

$$\langle \hat{\mathfrak{r}}_j \rangle_{mn} = (\hat{\mathfrak{r}}_j)_{mn} \, e^{-2k_{z,m}^{(j+1)} k_{z,n}^{(j)} \sigma_j^2} \qquad \langle \hat{\mathfrak{t}}_j \rangle_{mn} = (\hat{\mathfrak{t}}_j)_{mn} \, e^{(k_{z,m}^{(j+1)} - k_{z,n}^{(j)})^2 \sigma_j^2} \ . \tag{12}$$

These coefficients are formally similar to those for planar multilayers where the specular reflectivity is damped by the well-known damping exponential factors [9]

$$\langle \hat{\mathfrak{r}}_j \rangle = \hat{\mathfrak{r}}_j \, e^{-2k_z^{(j+1)} k_z^{(j)} \sigma_j^2} \qquad \langle \hat{\mathfrak{t}}_j \rangle = \hat{\mathfrak{t}}_j \, e^{(k_z^{(j+1)} - k_z^{(j)})^2 \sigma_j^2} \ . \tag{13}$$

By the dynamical theory, we can explain the roughness phenomena which are not observed in the reflectivity from planar multilayers such as the decrease of the scattered intensity for the incidence angle below the critical angle for the total external reflection or different sensitivity to the surface and interface roughnesses for strong and weak GTRs.

The above described procedure gives the intensity distribution along the GTRs of a multilayer grating with rectangular shape profile. Further discussion of the effect of the grating shape and grating roughness on the GTRs as well as comparison with the kinematical theory is given in [6,7,9].

4   Preparation procedures

There are two principal steps in the preparation of multilayer gratings — deposition of a multilayer and patterning providing the grating shape. In the previous text we discussed lamellar (or amplitude) gratings where deposition precedes patterning but in some cases the deposition is done on an already patterned substrate (phase gratings). The deposition is mostly performed by electron-beam evaporation in ultra-high vacuum or by sputtering, two kinds of the layers being deposited alternatively. The patterning mask is prepared by electron beam lithography or by optical holography. In the latter method a two-step procedure is usually used. The first (larger) mask is prepared by light exposure followed by wet chemical etching. Consequently, it is used to produce the final mask by UV lithography. Electron beam lithography is more time consuming but allows to prepare a larger variety of patterned structures, not only gratings. In both cases, reactive or non-reactive ion beam etching is used to obtain the final grating shape.

In the following, two multilayer gratings are presented. The planar multilayer was prepared in UMS 500 Balzers apparatus by electron beam evaporation on an oxidized Si(100) wafer with

a 0.3 μm thick SiO_2 passivation layer. Ten bilayers were deposited at the rate of 0.05 nm/s by alternating deposition of Si (nominal thickness 7 nm) and W (1 nm), Si being the first deposited layer. The layer thickness was controlled by a quartz monitor. The vacuum prior to the deposition 10^{-7} Pa decreased to 10^{-6} Pa and the substrate temperature increased to 50 °C during the deposition. Before further processing, the quality of the multilayer was checked by measuring the specular hard X-ray reflectivity with CuK_α radiation. A multilayer period of (7.8 ± 0.08) nm was found. The internal structure of the individual layers was found to be amorphous by X-ray diffraction. Therefore, any X-ray structural characterization of the subsequently prepared multilayer gratings was confined to the vicinity of the total external reflection region.

Electron-beam lithography was used to create lamellar grating structure. Both gratings were prepared from the same planar multilayer. A 300 nm thick layer of DuPont Elvacite 2041 PMMA resist was spin coated on the multilayer surface. The lithography was performed using a modified ZBA 10/1 direct-write vector-scan pattern generator (Carl Zeiss) with 30 kV accelerating voltage, the minimum spot size and deflection being 25 nm and 50 nm, respectively. The exposure was made by rectangular shots of 5 μm$\times$300 nm with a base dose of 600 μC/cm^2, using a combined dose/geometrical proximity correction. A 1 mm$\times$1 mm periodic array of 1 mm long and 300 nm wide lines was created shot by shot always in one direction (up-down) in one exposure cycle (without moving the sample), the line repetition period being 800 nm. For the sample No. 1, this procedure was done once with a given exposure time. For the sample No. 2, this procedure was done twice with a half exposure time each, the connecting points of the rectangular spots 5 μm$\times$300 nm along the line being shifted at the second exposure. The motivation was to suppress local heating effects and to obtain smoother walls of the grooves. For each sample, a resulting resist mask of the total area 5 mm$\times$5 mm corresponding to a grating with the lamella width and lateral period of 500 nm and 800 nm (1250 lamellae/mm), respectively, was achieved by sequential repositioning the sample. The final grating structure was obtained by Ar^+ ion beam etching (LPA USI Model Ionic) across the whole multilayer up to the substrate kept at 15 °C with a current density of 0.35 mA/cm^2 in a vacuum of 10^{-3} Pa. The residual resist was removed by standard wet and dry procedures.

5   X-ray structural characterization

A proper structural characterization of multilayer gratings is necessary to optimize the fabrication process and to understand their physical behaviour. Local probing methods such as atomic force or scanning electron microscopies represent a direct way of visualizing the surface profile. They are complementary to the X-ray scattering which probes locally the reciprocal space thus providing the information on structural parameters averaged over a large sample volume. Moreover, it is a non-destructive method of examining the quality of internal interfaces. The hard X-rays provided by common laboratory sources ($\lambda = 0.1 - 0.2$ nm) are advantageously used to measure specular and non-specular reflectivities (GTRs) by multilayer gratings.

At first, we inspected the samples by the atomic force microscopy and scanning electron microscopy (low-voltage field-emission Hitachi S 800), see Fig. 3. Such a test gives the first information whether the sample should be rejected or not. We found that the stitching accuracy of the 1 mm$\times$1 mm arrays exposed at fixed sample positions was kept below 100 nm in the sample No. 1 which exhibited a fairly regular grating shape. Contrary to the expectations, the

<center>(a)   (b)</center>
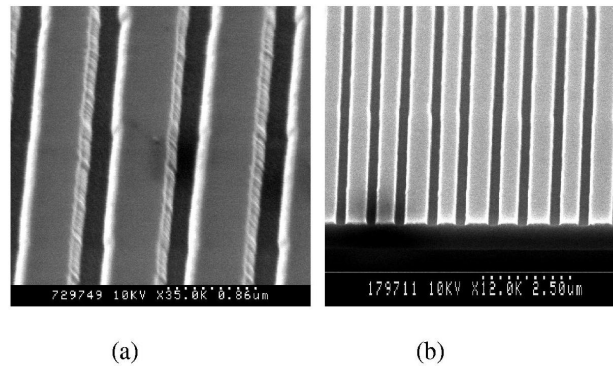
Fig. 3. Scanning electron microscopy photographs (a) top view (M=35 000) and (b) side view (cross section, M=12 000) which document the grating shape of the sample No. 1. Side wall roughness is observable, too.

sample No. 2 was worse. Therefore we chose the sample No. 1 for a more detailed study.

The X-ray measurements were done on a laboratory-made four-circle diffractometer. CuK$_\alpha$ radiation ($\lambda = 0.15418$ nm) provided by a Rigaku 12 kW rotating anode generator was monochromatized by a graphite monochromator and limited to a 50 μm wide beam by a slit. A NaI(Tl) scintillation detector was used with a slit of 80 μm. The measurements were performed in the coplanar geometry (the plane given by the incoming and detected beams was perpendicular to the mean sample surface) and with the lamellae perpendicular to the incoming beam (sample azimuth $\varphi = 90°$). By decreasing φ, the effective grating period D "seen" by the X-rays in the coplanar geometry would increase, being infinite (i.e. no grating diffractions observed) for $\varphi = 0°$ (lamellae along the incoming beam). In this case, the fan of grating diffractions stretches around the specular reflection out of the plane given by the incoming and specularly reflected beams. This fan may be measured only in a non-coplanar scattering geometry, e.g. with a two-dimensional position sensitive detector placed perpendicularly to the incident beam.

The specular reflectivity (GTR 0) was measured at first (Fig. 4). Larger peaks are the Bragg maxima located at the positions obeying Eq. (2) and smaller ones in between are Kiessig fringes originating from the interferences between the waves reflected from the surface and the multilayer/substrate interface. All these modulations are principally the same as for the planar multilayer. However, due to a smaller average density of the etched multilayer (smaller value), they are shifted downwards along the Q_z axis. The rocking curves measured with the detector fixed at the second Bragg order and the sample moving are shown for both samples in Fig. 5. The corresponding scan trajectories in the reciprocal space are indicated in Fig. 2. There are sharp peaks located symmetrically around the specular one (GTR 0) which originate from the intersection of the scan trajectory with the GTRs of positive and negative orders. A shape difference between the corresponding plus and minus GTRs comes only from the experimental resolution window (angular width of the detector multiplied by entrance divergence) which is not rectangular but slanted in the reciprocal space. Smaller peaks between the GTRs indicate a parasitic lateral superperiodicity which is double (sample No. 1) or even triple (sample No. 2) of the regular grating period. On closer inspection of the microscopic picture of the sample No. 1 (Fig. 3) it may be seen that every second lamella is slightly narrower (by less than 5 percent). A similar effect was
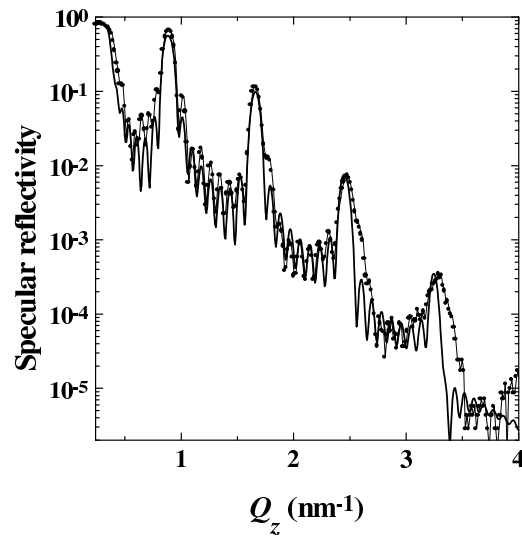
Fig. 4. Measurement (thin line with points) and simulation (thick line) of the specular reflectivity (GTR 0) of the sample No. 1. Bragg maxima and Kiessig fringes are well resolved.
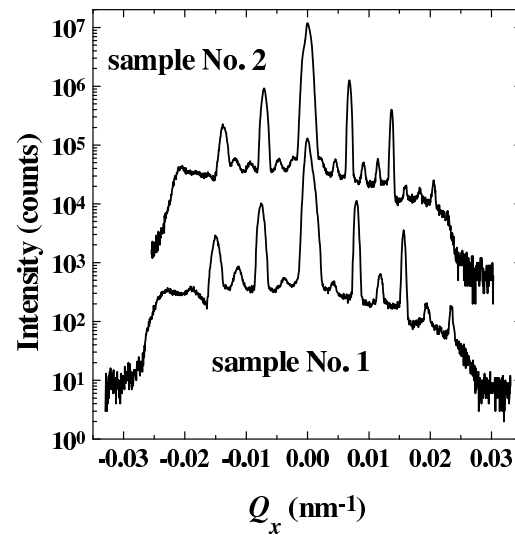
Fig. 5. Rocking curves measured across the second Bragg point (see Fig. 2). The side peaks come from the intersection of the scan trajectory with regular and parasitic GTRs (see the text). The broad background is due to the resonant diffuse scattering. The rocking curve of the sample No. 2 is shifted upwards by a factor of 10^2 because of clarity.

observed also in the sample No. 2 where two broader lamellae alternate with a narrower one. These features are caused by secondary effects of the patterning procedure like local heating effect and, though being subtle, may be revealed by the X-ray scattering very easily.
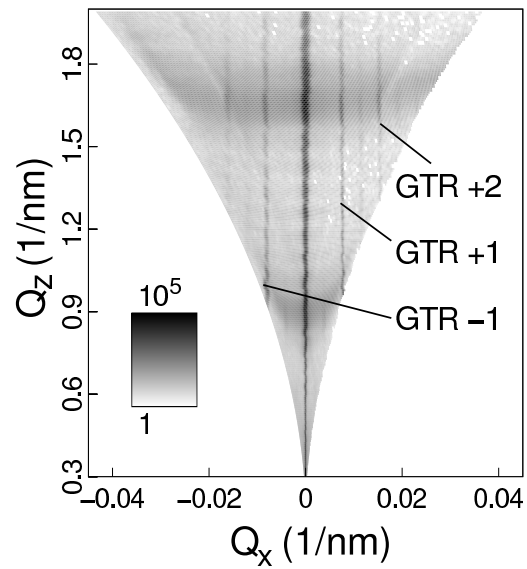
Fig. 6. Measured reciprocal space map of the sample No. 1. Both the GTRs and "bananas" of the resonant diffuse scattering are observable.
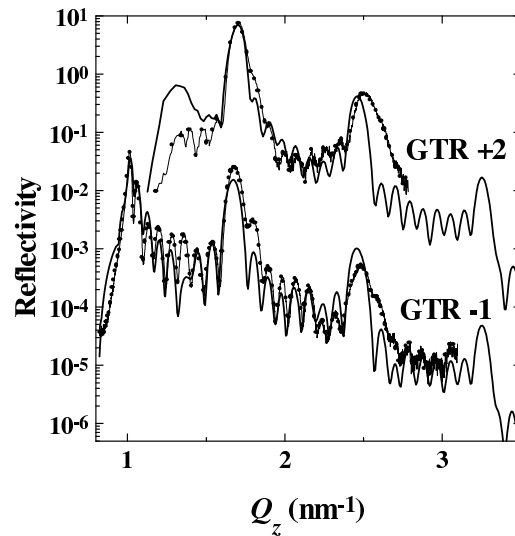
Fig. 7. Measurements (thin lines with points) and simulations (thick lines) of the GTR -1 and GTR $+2$ of the sample No. 1. The modulations copy those in the GTR 0. The curve GTR $+2$ is shifted upwards by a factor of 10^3 because of clarity.

A broad background in the rocking curves is the resonant diffuse scattering which comes from the interference of the waves scattered on rough but at least partially conformal interfaces of the multilayer [1]. It is concentrated into the banana-shaped regions around the multilayer

Bragg points in the reciprocal space (Fig. 2). Such "bananas" are directly observable in the measured reciprocal space map together with the GTRs (Fig. 6). The GTRs of non-zero orders were measured also separately (Fig. 7) with the sample and detector moving in such a way that the grating rule given by Eq. (1) was permanently fulfilled (the scan trajectory was along a GTR). The GTRs measured in this way were fitted within the dynamical theory to extract the basic structural parameters of the multilayer grating.

6 Quantitative analysis of X-ray measurements

The theory outlined previously is usable not only for the theoretical calculation of the multilayer grating efficiency at the working wavelength but also for the extraction of real structural parameters of the sample by hard X-rays. At first it has to be noted that the Q_z profiles of the corresponding GTRs of opposite orders are equal (within the experimental precision) which implies a weak multiple scattering among the GTRs without strong dynamical effects [6,7]. Further it follows from the dynamical theory of X-ray scattering for rough multilayer gratings that for the given wavelength and grating period, no multiple scattering effects among the GTRs are distinguishable in the GTR 0. Therefore specular reflectivity could be calculated as the reflectivity from a laterally averaged planar multilayer using Fresnel formalism (see e.g. [1]). The multilayer period determined from the simulation (Fig. 4) is $d = (7.73 \pm 0.07)$ nm which compares well with the multilayer period $d = (7.8 \pm 0.08)$ nm before patterning. A broadening of the third and fourth Bragg peaks may be attributed to the layer thickness fluctuations. The presence of seven Kiessig fringes instead of eight between two subsequent Bragg peaks, as it was the case before patterning, indicates a reduction of the uppermost multilayer period which is due to a tungsten oxide layer formation in the air. This layer was mechanically removed and/or thermally evaporated during an oxygen plasma treatment which was applied as the last step of the cleaning procedure to remove the resist from the grooves. Tungsten oxides have a low mechanical compatibility and some of them are volatile at elevated temperatures [10].

According to the kinematical theory of X-ray scattering, the lamella width to the grating period ratio affects the intensity modulations of the GTRs of different orders at a constant Q_z value while the ratio of the W and Si layer thicknesses controls (together with the interface roughness) the intensity modulations along each GTR. Both ratios determine the average density of the multilayer grating which controls the position of the maximum of the transmission function of the incident wave. This maximum is visible as the first sharp peak on the GTRs of non-zero orders and is represented by the critical angle for the total external reflection on the GTR 0.

The positions of the GTRs in the rocking curves (Fig. 5) obey Eq. (1) and provide a lateral period $D = 780$ nm which is close to the nominal value 800 nm. The measured GTRs up to the second order were simulated within the dynamical theory by fitting the structural parameters of the sample (Fig. 7). The background due to the resonant diffuse scattering is by one order or more below the intensity of the GTRs and was neglected (coherent scattering approximation). All GTRs were simulated simultaneously unless the mutual agreement of the simulated curves for the same set of fitted parameters was achieved. We obtained the layer thicknesses $d_{Si} = (6.23 \pm 0.07)$ nm and $d_W = (1.5 \pm 0.07)$ nm, the thickness of the uppermost W layer was (0.43 ± 0.3) nm, and the lamella width to the grating period ratio was (0.7 ± 0.08). The fitted parameters of the surface and interface roughness (0.58 ± 0.05) nm and (0.43 ± 0.07) nm, respectively, damped

considerably the reflected intensity at higher Q_z values far from the region of the total external reflection. Therefore the application of the dynamical theory including roughness was inevitable to obtain satisfactory simulations. Contrarily, the low-order GTRs are much less sensitive to the side wall roughness [6]. It was estimated to be 5 nm from the scanning electron microscopy (Fig. 3).

7   Conclusions

A brief overview of the technology and operation principles of multilayer gratings for the X-UV region was presented. A constant dispersion angle in a broad spectral range is their important property which facilitates the design of the optical elements based on multilayer gratings. The positions of multilayer grating diffractions are well described within the kinematical theory of X-ray scattering but their intensities are accessible only by the dynamical approach which includes multiple scattering effects among the GTRs of different orders. Two differently patterned lamellar gratings with the same nominal periods were exemplified. The mask exposition procedure was found to be decisive for achieving a regular grating pattern. It was shown that the hard X-ray specular and non-specular reflectivities may be used for extracting real structural parameters, both vertical and lateral, in a non-destructive way. This technique is applicable also to other types of mesoscopic structures studied in connection with new phenomena in magnetism, superconductivity and electronic transport. It is complementary to the microscopy methods which provide local and direct visualization of the surface. Further work should be concentrated on the relationship between the parameters of the real grating structure and the grating performance tested at the working wavelength.

References

[1]   M. Jergel, E.Majková, Š. Luby, R. Senderák, V. Holý: *Acta Phys. Slovaca* **48** (1998) 427

[2]   P. Dhez: *Ann. Physique* **15** (1990) 493

[3]   T.W. Barbee Jr., J.V. Bixler, D.D. Dietrich: *Physica Scripta* **41** (1990) 740

[4]   A. Sammar, J.M. André, B. Pardo: *Optics Commun.* **86** (1991) 245

[5]   F. Abèles: *Ann. Physique* **5** (1950) 596

[6]   P. Mikulík: *Ph.D. Thesis*, Université Joseph Fourier, Grenoble, and Masaryk University, Brno, 1997

[7]   P. Mikulík, T. Baumbach: *Phys. Rev. B* **59** (1999) 7632

[8]   M. Born and E. Wolf: *Principles of Optics* Pergamon Press, 1993

[9]   T. Baumbach and P. Mikulík: in *X-Ray and Neutron Reflectivity: Principles and Applications*, edited by J. Daillant and A. Gibaud, Lectures Notes in Physics, Springer, Berlin, 1999

[10] J.W. Mellor: *A Comprehensive Treatise on Inorganic and Theoretical Chemistry*, Vol. XI, Longmans & Green and Co., London, 1931, p. 753